Preparation and Testing of a Miniature High-Frequency Pulsed X-Ray Tube Based on Carbon Nanotube Cold Cathode

Kang Wang, Yunpeng Liu, Xiushan Wang, Menglai Tao, and Xiaobin Tang

***Abstract*—In this study, a compact high-frequency pulsed X-ray tube based on carbon nanotube (CNT) field emission was developed. A high-adhesion CNT cathode electron emitter was fabricated using an optimized slurry method and a grooved metal substrate, resulting in improved emission stability. The cathode exhibited a turn-on field of 1.78 V/μm, a field enhancement factor of 6014, and current fluctuations of less than 4% after conditioning. A miniature X-ray tube prototype with a diameter of 15 mm and a height of 47 mm was built in a dynamic vacuum environment. The pulse characteristics, imaging performance, and X-ray communication capabilities are all evaluated. The prototype achieved an amplitude-frequency response bandwidth of 1.05 MHz at 3 dB. The imaging showed a minimum focal spot size (FSS) of 0.879 $\times$ 1.153 mm, and high-speed imaging confirmed motion artifact suppression at pulse widths down to 300 μs. Reliable X-ray data transmission was demonstrated at data rates ranging from 1 to 6 Mbps, with PRBS7 encoding and bit error rates (BERs) below 10^{-3}. These results highlight the device's potential for high-speed imaging, low-dose diagnostics, and X-ray communication.**

***Index Terms*—Carbon nanotube (CNT) cathode, field emission miniature X-ray tube, high-speed imaging, pulsed emission, X-ray communication.**

I. Introduction

PULSED X-ray tubes emit short X-ray pulses with repetitive frequencies or arbitrary modulation. To meet various experimental and application requirements, the frequency, width, amplitude, and waveform of pulsed X-rays can be modulated by adjusting the behavior of electrons or X-rays in the X-ray tube [1]. Pulsed X-ray tubes offer low imaging artifacts, reduced radiation dose, and low power consumption, and have a wide range of applications, including laser additive manufacturing monitoring [2], high-speed X-ray imaging [3], distributed pulsed X-ray systems [4], X-ray elastography [5], and X-ray communication. Currently, pulsed X-ray tubes can be categorized according to their cathode type into grid-controlled hot cathode [6], [7], photo-controlled photocathodes [8], [9], [10], and field-emission cold cathodes [11], [12]. Field emission pulsed X-ray tubes based on cold cathodes have attracted considerable attention owing to their distinct advantages, including rapid switching, high resolution, digital operation, small focal spot size (FSS), and low power consumption [13]. These devices use field-emission electron tubes with various emission materials, including semiconductor tips [14], carbon nanotubes (CNTs), and other nanostructured carbon materials. CNTs have emerged as one of the most promising candidates for field-emission cathodes because of their high aspect ratio, excellent electrical conductivity [15], nanoscale diameter, high mechanical and electrical strength, and excellent chemical and thermal stability, making them ideal for field-emission applications [16]. Field emission, which extracts electrons directly under a strong electric field without thermal excitation, allows for the removal of heating components, reducing the X-ray tube size by more than 50%. Despite the significant advances in the development of CNT-based field-emission cathodes, several challenges remain in their practical deployment in digital X-ray tubes [17]. One of the most critical problems is the poor adhesion between CNTs and the metal substrate [18]. This limitation is primarily because of CNTs' chemical inertness, which results in poor interfacial bonding and adversely affects the long-term emission stability of field emission devices. In addition, most current field emission high-frequency X-ray tubes have frequencies below kilohertz, and there has been few researches into higher-frequency pulse emission [19]. The previous work mainly proposed a method for loading field emission cathode pulse voltage, achieved the emission of MHz field emission cathode pulse X-rays, and explored its feasibility for X-ray communication. Based on the previous work, this article has undergone further in-depth research. This article mainly studies cathode preparation, the construction of an X-ray tube prototype and its performance test.

This study proposes a compact cold cathode X-ray tube based on CNT field emission and high-frequency pulsed

Received 4 September 2025; revised 12 October 2025; accepted 13 October 2025. Date of publication 17 October 2025; date of current version 17 November 2025. This work was supported in part by the National Natural Science Foundation of China under Grant 12375256 and in part by the Postgraduate Research and Practice Innovation Program of Nanjing University of Aeronautics and Astronautics (NUAA) under Grant xcxjh20240609. *(Corresponding author: Yunpeng Liu.)*

Kang Wang, Xiushan Wang, and Menglai Tao are with the Department of Nuclear Science and Technology, Nanjing University of Aeronautics and Astronautics, Nanjing 210016, China.

Yunpeng Liu and Xiaobin Tang are with the Department of Nuclear Science and Technology, Nanjing University of Aeronautics and Astronautics, Nanjing 210016, China, and also with the Key Laboratory of Advanced Nuclear Technology and Radiation Protection, Ministry of Industry and Information Technology, Nanjing 210016, China (e-mail: liuyp@nuaa.edu.cn; tangxiaobin@nuaa.edu.cn).

Color versions of one or more figures in this article are available at https://doi.org/10.1109/TNS.2025.3622586.

Digital Object Identifier 10.1109/TNS.2025.3622586

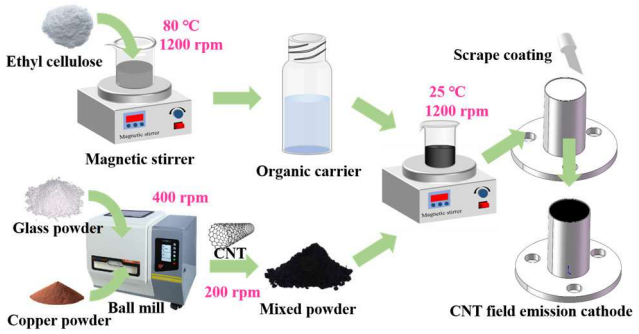

Fig. 1. CNT field emission cathode preparation process.

operation. To improve cathode lifetime and emission stability, an improved CNT slurry formulation and a recessed metal substrate were used to strengthen the adhesion between the CNTs and substrate. High-frequency pulsed voltages were applied to the cathode using an arbitrary waveform generator (AWG) and a power amplifier, allowing for high-speed imaging and X-ray communication experiments. A proof-of-concept prototype was constructed using a dynamic vacuum system, and its performance was experimentally validated. The proposed design provides valuable insights into the miniaturization of X-ray tubes, the extension of cathode service life, and the implementation of pulsed emission in advanced applications. This study aims to develop a miniature high-frequency pulsed X-ray tube based on CNT cold cathodes with enhanced emission stability, and makes the following contributions: an optimized CNT slurry process integrated with grooved substrates for superior interfacial bonding, a compact tube achieving record 1.05 MHz pulse bandwidth for CNT-based systems, and the first demonstration of motion artifact-free imaging with a pulsewidth of 300 μs and 6 Mbps X-ray communication capability were demonstrated for the first time.

II. Preparation and Characterization of the CNT Cold Cathode

A. Cathode Preparation

This experiment used industrial-grade multi-walled CNTs (MWCNTs) with an outer diameter of <10 nm and a length of 5–15 μm as electron emitters. To effectively disperse the functional phase, binder phase, and organic carrier whereas ensuring the reproducibility of a highly uniform and adhesive CNT paste for field electron emission applications, we introduced a process combining ball milling and magnetic stirring (see Fig. 1). Grooves were fabricated on the metal substrate to increase the contact area between the paste and substrate. Consequently, CNT emitters were obtained through high-vacuum annealing. In brief, 0.11 g of copper powder and 0.36 g of commercial glass powder were uniformly dispersed using ball milling at 400 r/min for 120 min. Subsequently, 0.15 g of CNTs was added to the mixture, followed by ball milling at 250 r/min for 40 min to achieve a uniform dispersion. Thereafter, ethyl cellulose (0.2 g) and terpineol (4 g) were mixed using a magnetic stirrer at 80 °C and stirred at 1200 r/min for 30 min to prepare the organic carrier. After cooling to 25 °C, the previously obtained powder mixture was added to the carrier and stirred for 60 min to form a homogeneous CNT paste. Importantly, the conductive copper powder improved the contact between CNTs and the substrate, increasing conductivity and facilitating electron transport during emission. Furthermore, the addition of inorganic glass powder as a binder improved the CNT cathode's the adhesion to the metal substrate, ensuring stable emission performance [20]. The CNT paste was blade-coated into grooves on a stainless-steel substrate with an opening diameter of 4.7 mm and a depth of 0.1 mm. The coated samples were dried in air at 90 °C for 120 min and then annealed at 300 °C in a high-vacuum chamber with a base pressure of 10^{-4} Pa. Finally, a CNT-cathode electron emitter was fabricated.

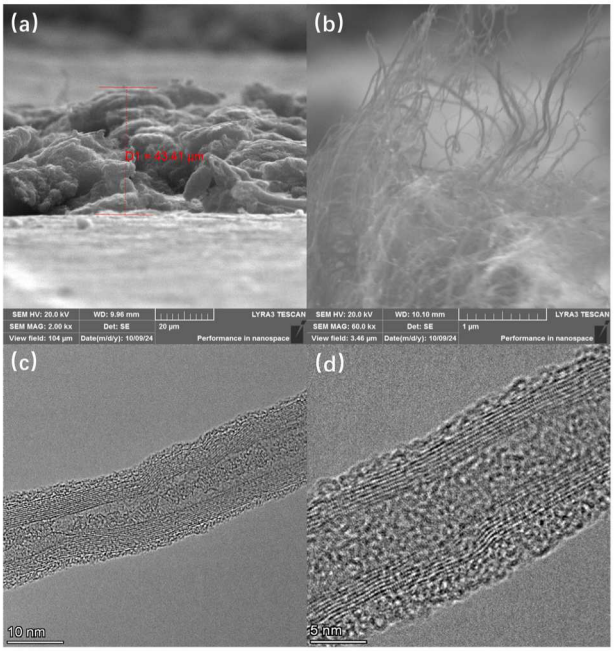

Fig. 2. Characterization of CNT cold cathode, (a) SEM scale bar = 20 μm; (b) SEM scale bar = 1 μm; (c) TEM scale bar = 10 nm; and (d) TEM scale bar = 5 nm.

B. Characterization and Performance Testing

The CNT cold cathode was characterized using scanning electron microscopy (SEM) and transmission electron microscopy (TEM), as shown in Fig. 2. The CNT filaments adhered well to the substrate and were predominantly aggregated on the surface protrusions. The CNTs exhibited random orientations, with most lying flat on the substrate. Only a small fraction extended outward, which was critical for effective electron emission. The diameter of the MWCNTs is approximately 10 nm, as shown in Fig. 2(c).

The electron emission characteristics of the CNT cathode were evaluated using a triode structure in which the cathode was grounded, the gate was biased at a constant voltage, and the anode was connected to a high voltage (U_{anode}). The cathode emission current increased exponentially with gate voltage (U_{Gate}), as shown in Fig. 3(a). The fabricated CNT

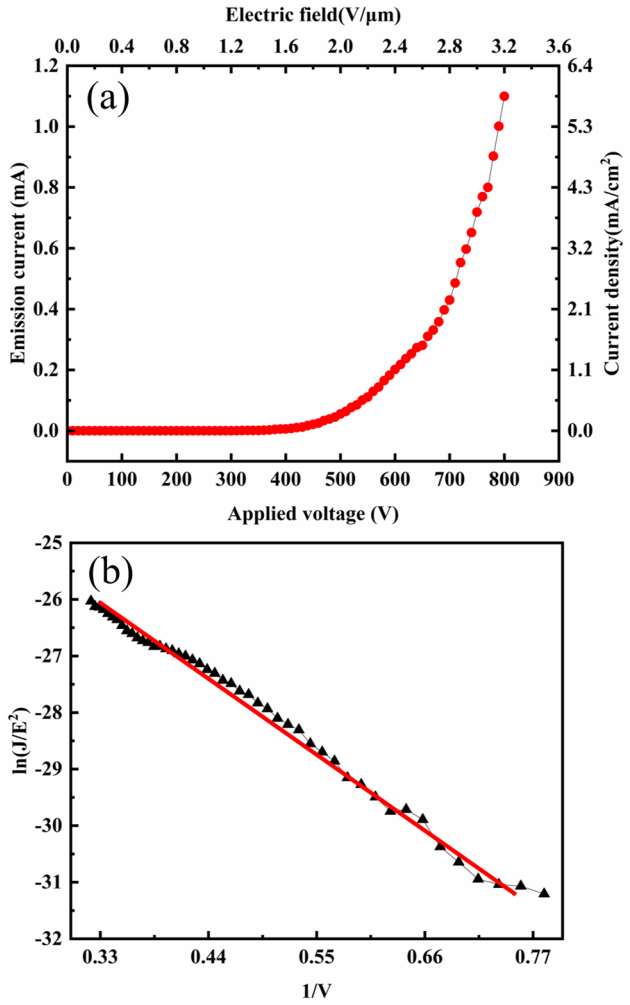

Fig. 3. Electron emission characteristics of CNT cold cathode, (a) I–V curve and (b) Fowler–Nordheim (F–N) theoretical verification.

cold cathode had a diameter of 4.88 mm. A gate with 200 μm square apertures and a copper anode mounted in a dynamic vacuum system were used. With a cathode–gate distance (D_{emi}) of 250 μm, an emission current of 0.1 mA was obtained at approximately 445 V, corresponding to a turn-on field of 1.78 V/μm. As the U_{Gate} increased, the cathode emission current increased exponentially. When the voltage is about 595 V, the emission current is 1 mA. The threshold electric field strength was 2.38 V/μm. When the U_{Gate} reached 800 V and had an electric field strength of 3.2 V/μm, the maximum measured emission current density was 5.879 mA/cm^2 owing to the limitation of vacuum conditions. This result is 7 times better than [21], attributed to the grooved substrate design concentrating electric fields on protruding CNTs.

According to the F–N formula

$$J = \frac{AE^2\beta^2}{\phi}\exp\left(-\frac{B\phi^{\frac{3}{2}}}{\beta E}\right). \tag{1}$$

After transformation

$$\ln\left(\frac{J}{E^2}\right) = -B\phi^{\frac{3}{2}}\frac{1}{\beta E} + \ln\left(\frac{A\beta^2}{\phi}\right) \tag{2}$$

where J denotes the current density, E denotes the cathode electric field strength, β denotes the field enhancement factor, and ϕ denotes the work function of CNT; here, ϕ = 5 eV [22] and A and B are constants. Equation (2) shows $\ln(J/E^2)$ and $1/E$ have a linear relationship. The linear relationship of I–V obtained from the experiment and transformed by the F–N formula is excellent, indicating that the cathode electron emission belongs to quantum tunneling. The field enhancement factor was calculated to be 6014 based on the slope of the F–N curve.

Following the J–E characteristic test, the cathode was subjected to 40 min of electrical aging at an initial current density of approximately 0.32 mA/cm^2 to remove CNTs with poor adhesion on the cathode surface and further activate the CNTs. During this process, only a small change in the current density was observed, indicating that the cathode was stable. Field emission stability tests were conducted after adjusting the voltage to maintain a current density at 0.32 mA/cm^2. The test results are shown in Fig. 4(a). The current fluctuation was calculated using (3) [23] as follows:

$$\delta_J = \frac{\sum_{i=1}^{N}\left|J_i - \overline{J}\right|}{N\overline{J}} \times 100\% \tag{3}$$

where J_i denotes the current density at each measurement point, $\overline{J}$ denotes the average current density, and N denotes the total number of measurement points. The average current fluctuation was 3.2%. These fluctuations are all less than 4%, indicating that the cathodes exhibit stable field emission properties. Compared with [24], the cathode electron emission did not decrease significantly after 40 min, while a significant decrease was observed in the literature, indicating that the cathode prepared by this cathode preparation method has good stability. This is mainly attributed to the fact that the addition of glass powder to the cathode slurry effectively improves the adhesion between the slurry and the metal substrate, and the surface grooves can effectively fix the CNTs on the surface for stable emission. The results of the micrometer scratch test are shown in Fig. 4(b). The graph shows that at a loading force of approximately 38.7 N, the CNT film may experience localized cracking or shedding. The results demonstrate excellent adhesion between the CNT film prepared using this method and the metal substrate.

III. Construction and Testing of the Miniature X-Ray Tube

A. Construction of the Miniature X-Ray Tube

A miniature X-ray tube prototype was constructed using the prepared CNT cathode. The device had a cylindrical structure with a diameter of 15 mm and a height of 47 mm. The D_{emi} was 250 μm. The focusing electrode used a dual-cylinder design with diameters of 12 and 10 mm, with the copper anode target was inclined at a 20° angle. The distance between the focusing electrode and the anode was approximately 10 mm. As shown in Fig. 5, the CNT cathode, gate mesh, focusing electrode, and anode were connected to the external equipment through electrode flanges.

The device operated in a dynamic vacuum system with a base pressure reaching as low as 1×10^{-7} Pa. During the

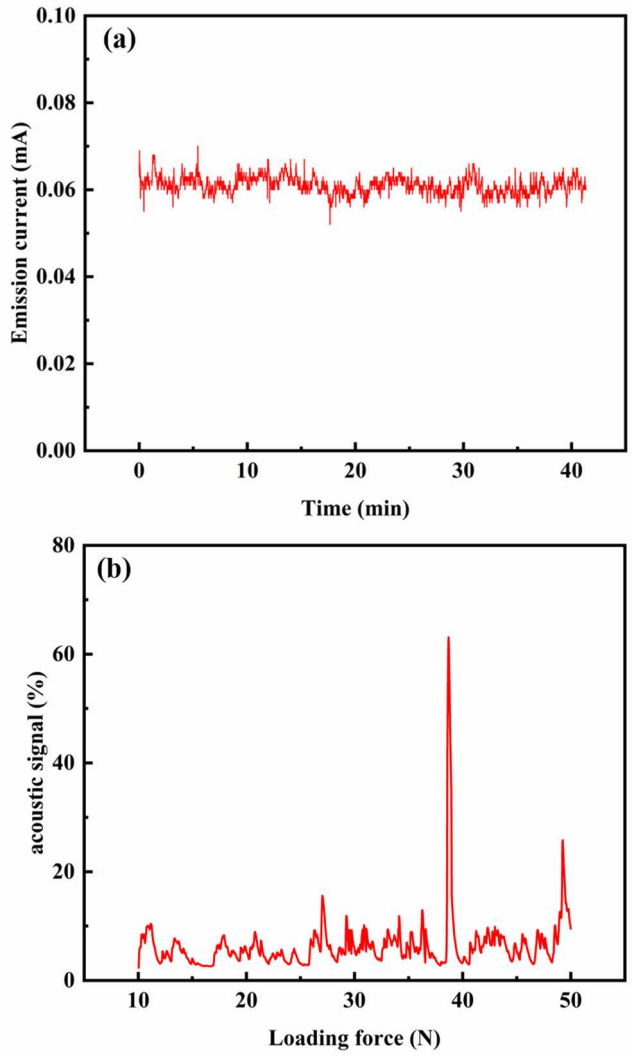

Fig. 4. (a) Field emission stability of cathodes and (b) micrometer scratch test.

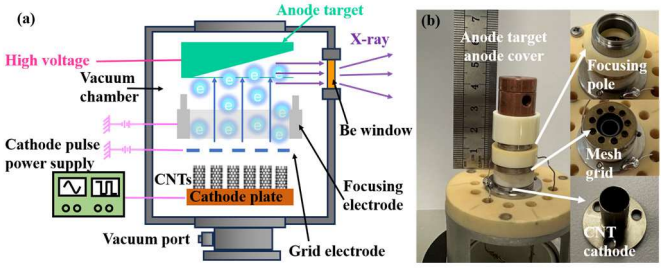

Fig. 5. (a) Schematic of the experimental setup and (b) photograph of the X-ray tube prototype.

whole experiment, the vacuum level was maintained below 1×10^{-5} Pa. Fig. 5(a) shows a schematic of the experimental setup and Fig. 5(b) shows a photograph of the X-ray tube prototype. High-frequency pulsed electron emission was achieved by modulating the voltage difference between the CNT cathode and the gate, which was controlled by an AWG and amplifier. The emitted electrons were then accelerated toward the anode to generate pulsed X-rays. It is important to note that when the cathode voltage is at a high level, the voltage difference between the cathode and gate is small, resulting in low electron emission and thus a low-level X-ray signal. Conversely, when the cathode voltage is low, a greater voltage difference induces stronger electron emission, corresponding to a high-level X-ray signal.

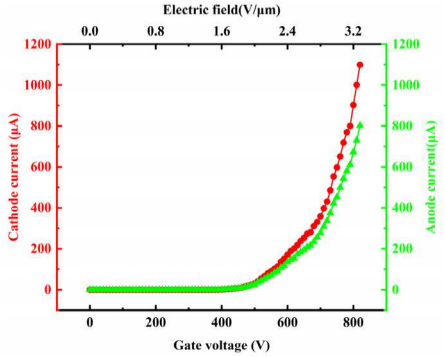

Fig. 6. Current testing of a compact X-ray tube prototype at an anode voltage of 10 kV, a focus voltage of 800 V, and a cathode-grid spacing of 250 μm.

B. Current Testing of the Miniature X-Ray Tube

When the U_{anode} was 10 kV and the focusing electrode voltage (U_{focus}) was 800 V, the variations of cathode and anode currents with different U_{Gate} are shown in Fig. 6. When U_{Gate} = 820 V, the cathode current reached 1.1 mA, and the corresponding anode current was 0.8 mA. The electronic pass rate was 72%. Because the addition of the focusing electrode and anode changed the surrounding electric field, the anode current in the prototype tube test was slightly lower than that in the CNT cathode test.

C. X-Ray Energy Spectrum and Dose Rate Testing

The tube's X-ray spectra were recorded at the U_{anode} between 20 and 35 kV using a compact integrated spectrometry system (XR-100SDD). As shown in Fig. 7(a), the characteristic K-series peaks of copper (Cu) were clearly observed in the spectra. The X-ray dose rate at a distance of 20 cm from the X-ray anode target (D_{at} = 20 cm) was measured for different U_{anode} values using the diagnostic X-ray measurement instrument RADCAL 10 × 6.6 M, as shown in Fig. 7(b), with the variation in the dose rate as a function of current. The results show a linear relationship between dose rate and current at the same U_{anode}.

D. X-Ray Pulse Emission Testing

To investigate the pulsed emission characteristics of the CNT cold cathode miniature X-ray tube, a sine wave signal with high and low levels of +5 and −5 V was generated using AWG. The signal frequency was then adjusted. This signal was amplified by a power amplifier (ATA-4315) with a fixed gain of 10 and then applied to the cathode, modulating electron emission and thus controlling pulsed X-ray generation. The X-ray detection system comprised a self-fabricated lutetium–yttrium oxyorthosilicate (LYSO)

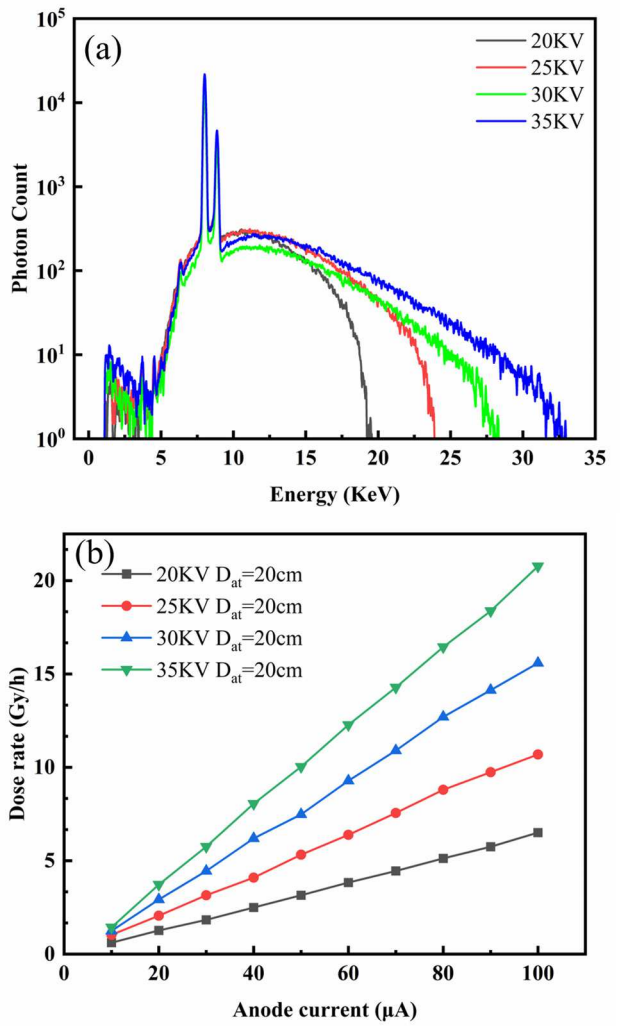

Fig. 7. (a) X-ray energy spectrum and (b) dose rate testing.

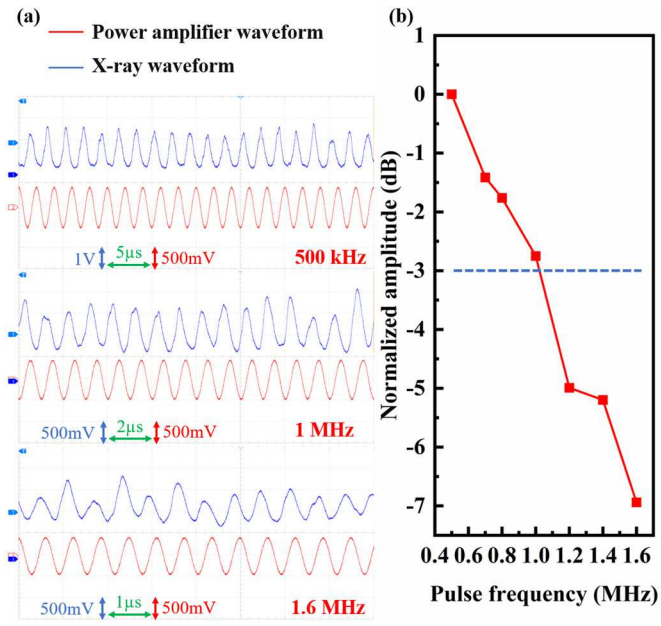

Fig. 8. Pulsed characteristics: (a) waveform and (b) amplitude-frequency response.

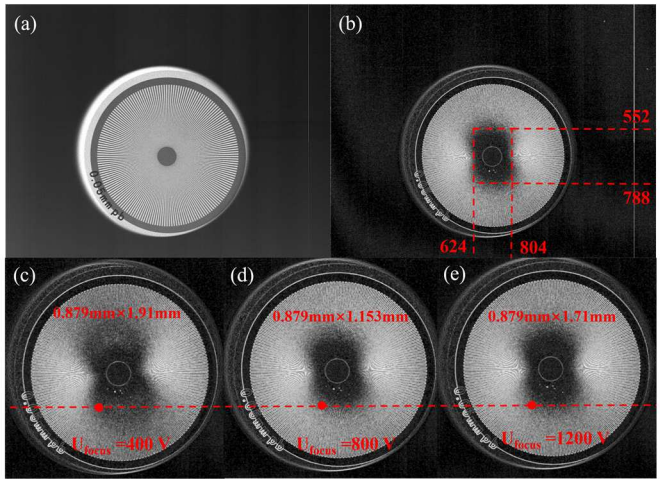

Fig. 9. (a) Star card image, (b) blurred region of star card image, and X-ray imaging blurred regions of star card at different focus voltages: (c) U_{focus} = 400 V; (d) U_{focus} = 800 V; and (e) U_{focus} = 1200 V.

scintillator coupled with a high-frequency-sensitive silicon photomultiplier (SiPM). A constant voltage of 590 V was applied to the gate, while the U_{focus} and U_{anode} of the X-ray tube were set to 800 V and 30 kV, respectively. The input signal's frequency was varied from 500 kHz to 1.6 MHz to obtain the X-ray pulse response. As shown in Fig. 8(a), the power amplifier's output waveform represents the modulation signal applied to the cathode, whereas the detected X-ray signal exhibits distinguishable high and low levels. According to the 3 dB bandwidth criterion, the normalized amplitude of the X-ray waveform was calculated as $20\ln(A/B)$, where A and B denote the X-ray signal amplitudes at the reference and target frequencies, respectively. As shown in Fig. 8(b), under the given operating conditions, the measured bandwidth of the CNT cold cathode miniature X-ray tube, when used as a communication signal transmitter, reached 1.05 MHz. This is basically consistent with the performance of previous work [25]. This amplitude-frequency response bandwidth nearly reached the highest frequency level reported to data. However, owing to the power amplifier's bandwidth limitation, the obtained frequency fell short of the limit of the developed X-ray tube prototype.

E. Focal Spot Test

To evaluate the imaging performance of the compact X-ray tube, imaging experiments were conducted using a star card (focal spot test card) with a flat-panel detector (Merak-1313, pixel size 100 μm). The experimental conditions were set with an U_{anode} of 30 kV, an anode current of 100 μA, and an exposure time of 10 s. The tube-to-object and tube-to-detector distances were 14 and 19 cm, respectively. The X-ray imaging effect was investigated under different focal electrode voltages, with the experimental results shown in Fig. 9. As shown in Fig. 9(c)–(e), the image quality transitioned from clear to blurry. The best imaging quality was observed at U_{focus} = 800 V, indicating that the optimal focusing voltage to achieve the smallest focal spot was approximately 800 V.

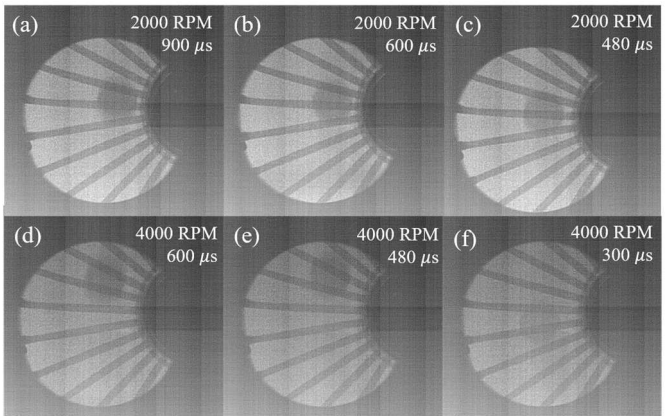

Fig. 10. High-speed imaging results of copper disk at a speed of 10.5 m/s with X-ray pulse widths of (a) 900, (b) 600, and (c) 480 μs, and at a speed of 31.5 m/s with X-ray pulse widths of (d) 600, (e) 480, and (f) 300 μs.

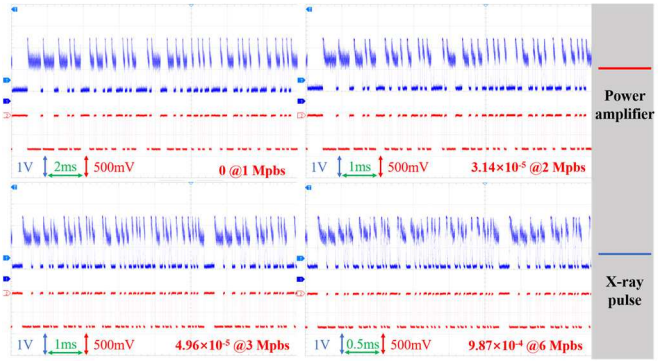

Fig. 11. Waveforms and BER of X-ray communication experiment.

The blurred region's size of was determined using the star card focal spot test method [26], as shown in Fig. 9(b). The minimum FSS was calculated to be 0.879 × 1.153 mm.

F. Applications in High-Speed Imaging and X-Ray Communication

To evaluate the compact X-ray tube's high-speed imaging performance, imaging experiments were conducted using a rotating fan with adjustable speed and a copper disk fixed in the center of each blade. The tube-to-object and tube-to-detector distances were set to 18 and 24 cm, respectively. The flat-panel detector was configured in the 2 × 2 binning mode with a frame rate of 100 Hz and synchronized with the compact X-ray tube prototype. The experimental conditions included an U_{anode} of 30 kV and a tube current of 40 μA. The effect of X-ray imaging was investigated at different fan speeds and X-ray pulse widths. As shown in Fig. 10(a)–(c), high-speed imaging results are displayed for a fan speed of 2000 r/min (copper disk speed of 10.5 m/s) at pulse widths of 900, 600, and 480 μs, respectively. As the pulsewidth decreases, so does the motion blur caused by the rotating copper disk. At a pulsewidth of 480 μs, the nut's profile becomes clearer. Fig. 10(d)–(f) shows the imaging results at a fan speed of 4000 r/min (copper disk speed of 20.9 m/s) for different X-ray pulse widths. At a pulsewidth of 480 μs, clear imaging was challenging; however, when the pulsewidth was reduced to 300 μs, the outline of the copper disk can still be clearly seen, but overall image clarity remained low because of the reduced X-ray intensity. The signal-to-noise ratio (SNR) of each image was calculated to be 3.55, 3.33, 3.25, 3.14, 3.09, and 2.91 dB for Fig. 10(a)–(f), respectively. When the pulsewidth is less than 300 μs, the image SNR is 2.91 dB, which is less than 3 dB, indicating a decrease in image clarity. However, owing to limitations in the flat-panel detector frame rate, the imaging rate is far from the limit of an X-ray tube, limiting high-speed imaging tests.

The X-ray communication experiment used a pseudorandom binary sequence (PRBS7), with an offline sampling of 200 000 bits for demodulation, resulting in bit error rates (BERs) at communication rates ranging from 1 to 6 Mbps. X-rays are also classified as particle-like entities. From an application perspective, statistical deviations in the amplitudes of such waveforms are of limited significance. Therefore, it is considered stable if the detector and its circuitry can distinguish the "1" signal of the X-ray. During the communication experiment, the U_{anode} was set to 30 kV and the U_{Gate} was 590 V, resulting in an anode current of 100 μA. Fig. 11 shows the power amplifier's output voltage and the square-wave waveform of the detected X-ray signal. The BER at 1 Mbps is 0, 3.14×10^{-5} at 2 Mbps, 4.96×10^{-5} at 3 Mbps, and 9.87×10^{-4} at 6 Mbps. These results indicate that the developed CNT cold cathode miniature pulsed X-ray tube supports X-ray communication at a speed of at least 6 Mbps, which is the best X-ray communication performance reported to date for CNT X-ray tubes [25], [27]. The BER increase at higher data rates is attributed to reduced X-ray photon density per bit and SiPM detector saturation effects. SNR degradation was observed above 4 Mbps due to pulse overlap at high rates. Improvements involve optimizing PRBS encoding or using photon-counting detectors.

IV. Conclusion

This study successfully developed a high-frequency pulsed miniature X-ray tube based on CNT cold cathodes, offering advantages such as a compact structure, fast response, stable emission, and clear imaging. The developed tube significantly increases the potential for X-ray applications in high-speed imaging and communication. The adhesion between the CNTs and the metal substrate was effectively improved using the ball milling-magnetic stirring process and the strategy of using recessed metal substrates, improving the conductivity and mechanical stability of the cathode and achieving excellent field emission performance. The test results show that the maximum emission current density reaches 5.879 mA/cm^2 at an applied electric field of 3.2 V/μm. The emission current fluctuation was maintained within 3.2%, indicating good current stability. The prototype of the developed miniature X-ray tube had a size of Φ15 × 47 mm, with clear X-ray energy spectrum characteristics and a pulse emission bandwidth up to 1.05 MHz, supporting adjustable X-ray output at different pulse frequencies. Imaging experiments showed that the optimal focal spot of 0.879 × 1.153 mm was achieved

at a focusing voltage of 800 V, allowing for clear imaging of high-speed moving targets with a minimum pulsewidth of 300 μs, effectively reducing motion artifacts and making it suitable for high-speed imaging scenarios. Furthermore, the system achieved a communication rate of up to 6 Mbps in X-ray communication tests, indicating its exploratory application value. This X-ray tube has significant potential for improving X-ray communication and high-speed X-ray imaging fields. This tube shows promise for portable medical diagnostics and industrial high-speed NDT. Current limitations include the flat-panel detector's frame rate (100 Hz), which restricts imaging to 100 fps despite the tube's MHz capability. Future work will integrate faster detectors and explore multiplexed communication schemes to overcome SNR barriers.

REFERENCES

[1] S. Lai, Y. Liu, J. Mu, Z. Feng, K. Miao, and X. Tang, "X-ray ultrashort pulse emission characteristic of carbon nanotube cold cathode X-ray source by pulse driving mode," *Vacuum*, vol. 207, Jan. 2023, Art. no. 111658, doi: 10.1016/j.vacuum.2022.111658.

[2] C. Zhao et al., "Real-time monitoring of laser powder bed fusion process using high-speed X-ray imaging and diffraction," *Sci. Rep.*, vol. 7, no. 1, p. 3602, Jun. 2017, doi: 10.1038/s41598-017-03761-2.

[3] H. Y. Choi, C. H. Shon, and J. U. Kim, "Development of new X-ray source based on carbon nanotube field emission and application to the non destructive imaging technology," *IEEE Trans. Nucl. Sci.*, vol. 56, no. 3, pp. 1297–1300, Jun. 2009, doi: 10.1109/TNS.2009.2012858.

[4] W. P. Leemans et al., "Interaction of relativistic electrons with ultrashort laser pulses: Generation of femtosecond X-rays and microprobing of electron beams," *IEEE J. Quantum Electron.*, vol. 33, no. 11, pp. 1925–1934, Nov. 1997, doi: 10.1109/3.641307.

[5] C. Kamezawa, A. Cramer, W. Krull, W. Yashiro, K. Hyodo, and R. Gupta, "Dynamic X-ray elastography using a pulsed photocathode source," *Sci. Rep.*, vol. 11, no. 1, p. 24128, Dec. 2021, doi: 10.1038/s41598-021-03221-y.

[6] Z. Feng, Y. Liu, J. Mu, W. Chen, S. Lai, and X. Tang, "Optimization and testing of groove-shaped grid-controlled modulated X-ray tube for X-ray communication," *Nucl. Instrum. Methods Phys. Res. A, Accel. Spectrom. Detect. Assoc. Equip.*, vol. 1026, Mar. 2022, Art. no. 166218, doi: 10.1016/j.nima.2021.166218.

[7] A. P. Gupta et al., "Compact X-ray tube with ceramic vacuum seal for portable and robust dental imaging," *IEEE Trans. Electron Devices*, vol. 68, no. 9, pp. 4705–4710, Sep. 2021, doi: 10.1109/TED.2021.3097315.

[8] S. Hang, Y. Liu, H. Li, X. Tang, and D. Chen, "Temporal characteristic analysis of laser-modulated pulsed X-ray source for space X-ray communication," *Nucl. Instrum. Methods Phys. Res. A, Accel. Spectrom. Detect. Assoc. Equip.*, vol. 887, pp. 18–26, Apr. 2018, doi: 10.1016/j.nima.2018.01.031.

[9] S. M. Foreman, C. Kealhofer, G. E. Skulason, B. B. Klopfer, and M. A. Kasevich, "Ultrafast microfocus X-ray source based on a femtosecond laser-triggered tip," *Annalen der Physik*, vol. 525, nos. 1–2, pp. L19–L22, Feb. 2013, doi: 10.1002/andp.201200186.

[10] H. Yu et al., "Design and testing of metal photocathode X-ray source based on microchannel plate," *IEEE Trans. Electron Devices*, vol. 71, no. 11, pp. 7099–7105, Nov. 2024, doi: 10.1109/TED.2024.3465463.

[11] L. Pirker, R. Ławrowski, R. Schreiner, M. Remškar, and B. Višić, "$Mo_xW_{x-1}S_2$ nanotubes for advanced field emission application," *Adv. Funct. Mater.*, vol. 33, no. 15, Apr. 2023, Art. no. 2213869, doi: 10.1002/adfm.202213869.

[12] Y. Ahn et al., "Overall control of field emission from carbon nanotube paste-emitters through macro-geometries for high-performance electron source applications," *Carbon*, vol. 189, pp. 519–529, Apr. 2022, doi: 10.1016/j.carbon.2021.12.094.

[13] S. H. Heo, H. J. Kim, J. M. Ha, and S. O. Cho, "A vacuum-sealed miniature X-ray tube based on carbon nanotube field emitters," *Nanosc. Res. Lett.*, vol. 7, no. 1, p. 258, Dec. 2012, doi: 10.1186/1556-276x-7-258.

[14] L. Dvorson, G. Sha, I. Kymissis, C.-Y. Hong, and A. Akinwande, "Electrical and optical characterization of field emitter tips with integrated vertically stacked focus," *IEEE Trans. Electron Devices*, vol. 50, no. 12, pp. 2548–2558, Dec. 2003, doi: 10.1109/TED.2003.819700.

[15] J.-W. Kim et al., "Electrostatic focusing lens module with large focusing capability in carbon nanotube emitter-based X-ray sources," *IEEE Electron Device Lett.*, vol. 36, no. 4, pp. 396–398, Apr. 2015, doi: 10.1109/LED.2015.2404874.

[16] J. S. Han, S. H. Lee, and C. J. Lee, "High-performance field electron emitters fabricated using a free-standing carbon nanotube film," *IEEE J. Electron Devices Soc.*, vol. 10, pp. 402–407, 2022, doi: 10.1109/JEDS.2022.3178742.

[17] J.-W. Jeong, J.-W. Kim, S. Choi, J.-T. Kang, and Y.-H. Song, "The vacuum-sealed micro-focus X-ray tube with CNT field emitters," in *Proc. IVESC*, Apr. 2012, pp. 93–94, doi: 10.1109/IVESC.2012.6264163.

[18] E. Go et al., "Enhanced interfacial reaction of silicon carbide fillers onto the metal substrate in carbon nanotube paste for reliable field electron emitters," *Nanotechnology*, vol. 32, no. 19, May 2021, Art. no. 190001, doi: 10.1088/1361-6528/abe1ef.

[19] S. Lai, X. Tang, Y. Liu, J. Mu, Z. Feng, and K. Miao, "X-ray high frequency pulse emission characteristic and application of CNT cold cathode X-ray source cathode X-ray source," *Nanotechnology*, vol. 33, no. 7, Feb. 2022, Art. no. 075201, doi: 10.1088/1361-6528/ac378b.

[20] J. Chen et al., "'Double-high' field electron emission of screen-printed carbon nanotube cathodes," *Vacuum*, vol. 217, Nov. 2023, Art. no. 112517, doi: 10.1016/j.vacuum.2023.112517.

[21] M. M. H. Raza et al., "Study the electron field emission properties of silver nanoparticles decorated carbon nanotubes-based cold-cathode field emitters via post-plasma treatment," *J. Mater. Sci., Mater. Electron.*, vol. 33, no. 9, pp. 7191–7211, Mar. 2022, doi: 10.1007/s10854-022-07900-y.

[22] Y. Zhang, S. Deng, J. Du, X. Lai, J. Chen, and N. Xu, "Effects of pulsewidth and area of carbon nanotube films on their pulsed field emission characteristics," *IEEE Trans. Electron Devices*, vol. 60, no. 8, pp. 2677–2681, Aug. 2013, doi: 10.1109/TED.2013.2270313.

[23] L. Wang et al., "Fabrication of large-area ZnO nanowire field emitter arrays by thermal oxidation for high-current application," *Appl. Surf. Sci.*, vol. 484, pp. 966–974, Aug. 2019, doi: 10.1016/j.apsusc.2019.04.169.

[24] Y. C. Choi et al., "Preparation of a miniature carbon nanotube paste emitter for very high resolution X-ray imaging," *Carbon*, vol. 100, pp. 302–308, Apr. 2016, doi: 10.1016/j.carbon.2016.01.026.

[25] Y. Li et al., "X-ray transmission effects in a high-density dynamic-dusty plasma environment," *Vacuum*, vol. 212, Jun. 2023, Art. no. 112260, doi: 10.1016/j.vacuum.2023.112260.

[26] J. D. Everson and J. E. Gray, "Focal-spot measurement: Comparison of slit, pinhole, and star resolution pattern techniques," *Radiology*, vol. 165, no. 1, pp. 261–264, Oct. 1987, doi: 10.1148/radiology.165.1.3628780.

[27] K. Miao et al., "Emission characteristics of pulse CNT cold cathode X-ray source combined with channel electron multiplier," *Appl. Radiat. Isot.*, vol. 206, Apr. 2024, Art. no. 111243, doi: 10.1016/j.apradiso.2024.111243.